THE JOURNAL OF PHYSICAL CHEMISTRY C
A JOURNAL OF THE AMERICAN CHEMICAL SOCIETY

pubs.acs.org/JPCC
Article

Impact of the Interfacial Thermal Conductance on the Thermoplasmonic Response of Metal/Polymer Hybrid Nanoparticles under Nanosecond Pulsed Illumination

Javier González-Colsa, Fernando Bresme,* and Pablo Albella*

Cite This: J. Phys. Chem. C 2023, 127, 19152−19158
Read Online

ABSTRACT: Janus nanoparticles containing plasmonic materials have attracted great attention in the thermoplasmonic community due to their potential for applications in thermoelectronics or biomedicine. A significant number of thermoplasmonic applications rely on the heating of nanostructures by using pulsed excitation lasers. The heating generated in these nanostructures is often transferred to other regions via material−fluid interfaces. This heat transfer dynamics is controlled by the interfacial thermal conductance. In this work, we investigate the impact of the interfacial thermal conductance on the thermal relaxation of metal−polymer Janus nanoparticles that generate directional heating under pulsed illumination. We show that neglecting the temperature dependence of the thermophysical properties results in an overestimation of the temperature of the nanoparticle. A gold/polymer semishell nanostructure was used as an example not only to illustrate the aforementioned effects but also to show it as a reliable nanoheater candidate for photothermal therapies, capable of offering a remarkable temperature increment and presenting directional heating. The model we developed here can be applied to any type of nanoarquitecture, showing this work as a powerful tool for topics beyond photothermal therapies that can contribute to the development of novel structures able to control heat on the nanoscale.

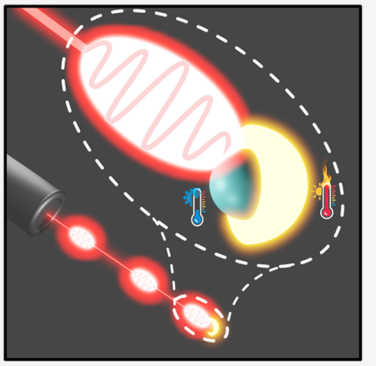

INTRODUCTION

Janus nanoparticles are hybrid structures composed of materials with contrasting physical and chemical properties. Since the first manufactured Janus nanoparticle (JNP),[1] the interest in this kind of structure has grown enormously in the past decades leading to the development of novel manufacturing techniques. Nowadays, Janus nanoparticles with heterogeneous composition (dielectric, magnetic orplasmonic, for instance), shapes, and sizes can be found in the literature. The contrasting properties of those particles lead to novel thermal transport mechanisms and thermophoretic responses,[2−4] which can be potentially exploited in biomedical applications such as hyperthermia. Hyperthermia promises to deliver medical treatments to target selectively the destruction in situ of cells inside our bodies.[5−7]

Among the existing family of JNPs, those incorporating plasmonic materials have attracted special attention in nanomedicine, due to their ability to efficiently generate[8,9] and control heat[10,11] at the nanoscale. Heating generation relies on the excitation of Localized Surface Plasmons Resonances (LSPRs), namely, electromagnetically driven coherent oscillations of free plasma in metallic nanoparticles.[12] At the LSPR frequency, the electronic motion is enhanced owing to the magnification of resistive losses which finally translates into a boosted heat generation.[13−15] An efficient heat generation platform can lead to substantial temperature increases of several 10s to 100s K above the solvent temperature. Therefore, thermoplasmonics is widely recognized as a powerful tool to develop novel hyperthermia approaches in nanomedicine.[5−7]

Very recently, we showed that JNPs built of materials with contrasting thermal conductivities can be used to generate heat asymmetrically under continuous wave excitation in the second biological spectral window ($\lambda \in [1000,1400]$ nm), opening a real possibility for its application in photothermal therapies (PTT).[11] However, it is known that most optically assisted therapies in biomedicine use pulsed lasers to avoid adverse effects on tissue.[16] This variable can be critical in thermoplasmonic calculations since their response depends on the pulse features. Furthermore, in that work, we did not consider the effect of the Interfacial Thermal Conductance (ITC), which influences the heat transfer across material−fluid interfaces. Neglecting ITC effects is justified in homogeneous nanoparticles at stationary conditions, if one is interested in the solvent temperature next to the particle, since this temperature is independent of the ITC.[17] For full theoretical treatment, one needs to include the ITC, as the temperature of the

Received: May 24, 2023
Revised: September 4, 2023
Published: September 14, 2023

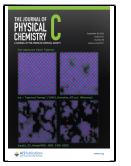

https://doi.org/10.1021/acs.jpcc.3c03514
J. Phys. Chem. C 2023, 127, 19152−19158

nanoparticle for a given illumination condition does depend on the ITC. Moreover, we demonstrated in ref 10 that Janus nanoparticles consisting of materials with very different hydrophobicity, generate anisotropic heat rates at stationary conditions. This physical effect can be exploited to induce anisotropic heating at the nanoparticle surface by modulating the interfacial thermal conductance of the JNPs. The investigation of nanoparticles with heterogeneous chemical composition must be performed including interfacial thermal conductance effects. In this work, we investigate the influence of the ITC on the transient heating and cooling of Janus plasmonic nanoparticles under nanosecond-pulsed illumination. Our JNPs mimic experimental systems and consist of a polymeric nanosphere coated with a gold spherical cap.

METHODS

We solved the heat diffusion equation using finite element methods (Comsol Multiphysics software). First, we solve Maxwell equations to calculate the JNP absorption cross section. This was done by considering a continuous plane wave exciting the nanoparticle immersed in bulk water surrounded by Perfectly Matched Layers (PMLs). Then, we computed the total power absorbed by the nanoparticle to calculate the absorption cross section. We also solve the Maxwell equations by finite difference time domain (FDTD) methods (Lumerical FDTD in this case) to double check the absorption value, by following a similar process and testing the convergence of the result by varying the mesh step (see Figure S1). Once the absorption calculation is converged, we solve the time dependent heat transfer equation considering that there are no changes of state using a Gaussian pulse excitation to set the power density $Q(t)$. This excitation aims to mimic the experimental irradiation conditions of a nanosecond pulsed laser. To model the Gaussian pulse, we follow ref 17 and use a normalized Gaussian envelope described by

$$p(t) = \frac{1}{\tau} e^{-\pi(t-t_0)^2/\tau^2} \tag{1}$$

where τ is the pulse duration and t_0 is the position of the temporal amplitude. The fluence F provides information on the performance of a pulsed laser and is defined by laser energy per unit area. The fluence has been used before in thermoplasmonics to quantify the threshold for bubble generation or structure fracture threshold, upon heating.[18,19] The total absorbed energy (q) by the JNP as a function of the fluence is defined by

$$q = \sigma_{\text{abs}} F \tag{2}$$

and the absorbed energy density (per volume unit) can be written as

$$\overline{q} = \frac{\sigma_{\text{abs}} F}{V} \tag{3}$$

where σ_{abs} is the JNP absorption cross section and V is the absorber volume. In our case, the absorber material is only the metallic part of the particle since the polymer does not absorb in the vis−NIR spectral range.[20] A typical laser mode is much larger than the nanoparticle and the simulation region; therefore, a plane wave can be considered to compute σ_{abs} (see Section I of the Supporting Information (SI)). Thus, the spatial dependence of $\overline{q}$ was intrinsically included in the absorption cross section calculations.

The metallic coating (see Figure 2) has a semispherical shape with volume $V = 2\pi/3((R+\delta)^3 - R^3)$, where R is the radius of the polymer sphere and δ is the gold layer thickness. We define the time dependent heat power density as follows:

$$Q(t) = \frac{3}{2\pi} \frac{\sigma_{abs} F}{((R+\delta)^3 - R^3)\tau} e^{-\pi(t-t_0)^2/\tau^2} \tag{4}$$

where $Q(t)$ is the instantaneous heat produced by the JNP at time t. $Q(t)$ is an input for the heat diffusion equation, whose solution is performed numerically to compute the time and spatial dependence of the temperature.

RESULTS AND DISCUSSION

To develop our model, we first tested our method for homogeneous nanoparticles against previous studies by Baffou et al.[17] In that work, the authors developed a numerical framework to solve the heating problem of homogeneous metallic nanoparticles immersed in water under pulsed illumination without considering changes of state. They showed that a 20 nm radius gold nanosphere can reach temperature increases of $\Delta T = 400$ °C for a fluence $F = 38$ J/m^2 using a Gaussian pulse defined by $\tau = 1$ ns and $t_0 = 2$ ns. We used these parameters for our analysis along with an ITC of $G_K = 150$ MW/(K m^2), as reported in ref 17. Recently, the ITC of gold−water interface was computed using molecular dynamics simulations and polarizable metallic surfaces, predicting values of $G_K = 200$ MW/(K m^2)[21] for gold temperatures of the order of 60 °C. We also performed calculations with this ITC. Advancing the discussion below, the higher thermal conductance results in a significant decrease of the temperature maximum.

Figure 1a shows the transient radial thermal profiles for a 20 nm radius gold nanosphere illuminated by a Gaussian pulse. We have considered the simulation region large enough as to allow for a complete thermal relaxation neglecting melting effects. Although gold may exhibit changes in shape and geometry due to premelting effects before reaching the melting temperature,[22] its stability can be preserved.[23] Indeed, no significant evidence of premelting has been reported at temperatures lower than 726 °C,[24] as this temperature is much higher than the one achieved in our illumination conditions. Red and yellow curves represent the time-dependent temperature of the Au particle bulk and the water in contact with the nanoparticle surface. Notice that our results agree with those obtained in ref 17 under the same conditions. The maximum temperature is reached at approximately 1 ns after the excitation pulse, and the ITC produces a temperature jump at the gold−water interface.

The thermoplasmonic heating results in a large temperature increase of the solvent, reaching values close to 300 °C. The thermal conductivity and specific heat of gold and water change significantly in the temperature range of 300−550 K. We have assessed the impact of these changes by including temperature dependent properties in the solution of the heat diffusion equation. In doing so, we kept the ITC constant for these calculations, since a weak dependence with temperature was recently reported by simulations of gold nanoparticles in water.[25] Thus, we used the temperature dependent thermal conductivities and specific heats provided in the material database of Comsol Multiphysics, which are extracted from ref 26. We show, in Figure 1b, the same calculations reported in panel **a**, but considering the temperature dependent thermal

https://doi.org/10.1021/acs.jpcc.3c03514
J. Phys. Chem. C 2023, 127, 19152−19158

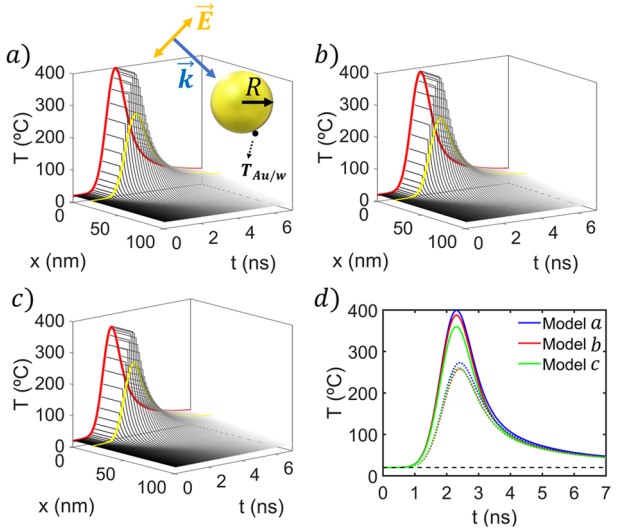

Figure 1. Transient thermal response of a 20 nm radius (R) gold sphere illuminated by a temporal Gaussian pulse with $F = 38\ \mathrm{J/m^2}$, $\tau = 1$ ns, and $t_0 = 2$ ns. Time evolution of the temperature profiles along the x axis (radial distance) for (a) gold−water ITC of $G_K = 150\ \frac{\mathrm{MW}}{\mathrm{m^2\ K}}$ and gold and water thermal conductivities independent of temperature ($k_w = 0.6\ \frac{\mathrm{W}}{\mathrm{mK}}$, $k_{Au} = 307.2\ \frac{\mathrm{W}}{\mathrm{m\ K}}$), (b) $G_K = 150\ \frac{\mathrm{MW}}{\mathrm{m^2\ K}}$ and temperature dependent thermal conductivities (see Figure S2 in the SI), and (c) $G_K = 200\ \frac{\mathrm{MW}}{\mathrm{m^2\ K}}$ taken from ref 21 and temperature dependent thermal conductivities. The red curve represents the time evolution of the temperature inside the gold, and the yellow one is the interfacial temperature corresponding to the temperature of the solvent at a radial distance of 0.1 nm from the gold surface ($T_{Au/w}$). (d) Time dependence of the temperature of the particle (continuous line) and solvent (dotted line) at the gold surface ($T_{Au/w}$). The color lines: blue, red, and green correspond to the models used in (a), (b), and (c), respectively. Upper inset: $\vec{E}$ and $\vec{k}$ represent the incident electric field and wavevector for a wavelength (λ = 532 nm), respectively.

properties. The water thermal properties were taken for a compressed fluid. Thus, the solvent does not experience any change of state along the studied temperature range. This allows a fair comparison with ref 17, where authors use constant thermophysical properties. The maximum temperature reached by the particle and the surrounding solvent decreases by approximately 15 K relative to the temperature obtained using constant thermophysical properties. The change in the temperature is mostly driven by changes in the heat capacity of water. Indeed, the isobaric density and thermal conductivity of both water and gold, and the specific heat of gold, feature a weak dependence with temperature (see Figure S2 in the SI). However, the specific heat of water does change from ∼4200 J/(kg·K) to ∼5200 J/(kg·K) for the case of $\Delta T \approx$ 280 K, from T = 273 K to T = 553 K. This means that water is progressively able to store more energy per temperature unit when it is heated, something that significantly affects the transient thermal process. This result underlines the need to include the temperature dependence of relevant thermophysical properties in the theoretical solution of the heat diffusion equation (especially for the water specific heat) to accurately describe the thermal transport processes at the nanoscale.

In Figure 1c, we investigate the impact of ITC on the transient heating/cooling process. These computations were performed using temperature dependent thermophysical properties. A higher ITC results in lower metal overheating since the metal−water interface features a lower thermal resistance. To compare all the cases investigated above, we show in Figure 1d the temporal evolution of the temperature at the center of the gold nanoparticle (continuous line) and at the gold water interface (dotted line) obtained from models a, b, and c. The maximum in the temperature of the nanoparticle exhibits a significant dependence with the ITC. Higher thermal conductance 200 vs 150 $\frac{\mathrm{MW}}{\mathrm{m^2\ K}}$ results in a substantial reduction of the maximum temperature achieved by the nanoparticle ($\Delta T \sim$ 40 K) after 1 ns. The temperature difference of the solvent at the particle surface also depends on the ITC, and we observe consistently a smaller temperature jump at the interface. These results highlight the importance of the ITC when investigating the transient thermal transport properties of nanomaterials. In fact, geometrical imperfections derived from the manufacturing processes, such as roughness or porosity, would enhance the ITC, as the surface−solvent coordination number would be even higher modifying the predicted thermal transport behaviour.

On the other hand, the temperature can also affect metal permittivity as reported in refs 27−31. To take this effect into account, we have modeled the gold permittivity as a Drude−

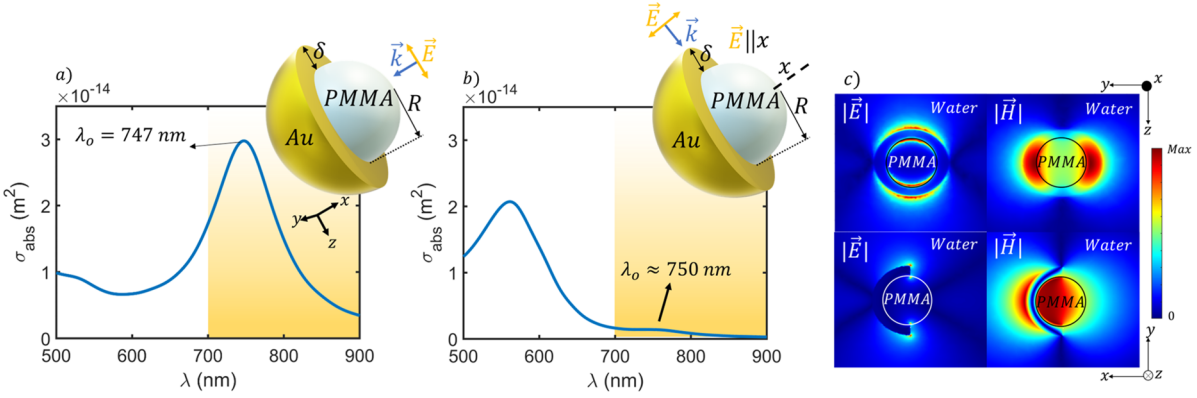

Figure 2. Absorption cross section of a polymer-gold semishell JNP with δ = 20 nm and R = 40 nm illuminated with the electric field polarized along the largest dimension of the nanocap (a) and along the shortest dimension (b). λ_0 is the resonance wavelength, and the orange area highlights the NIR-I. (c) xy and yz mapping of the electric and magnetic field enhancements for (a). Inset: Schematic of the JNP under illumination conditions.

https://doi.org/10.1021/acs.jpcc.3c03514
J. Phys. Chem. C 2023, 127, 19152−19158

Lorentz function where the Drude damping constant is temperature dependent[27,28] (see Section II of the Supporting Information). This model suggests the non-negligible variation of the optical constants with temperature, especially for high temperature increments. Figures S3 and S4 show how the temperature dependent Drude damping constant influences the gold permittivity. The imaginary part increases, being this change more prominent in the infrared, while the real part remains almost constant as already reported in the literature.[28] This leads to a reduction in the absorption efficiency and consequently to a temperature drop, as suggested in Figures S5, S6. Therefore, the expected temperature from model *c* will decrease from 360 to 330 °C, giving a reduction of ∼9%. Although it is a small relative change, it is non-negligible given the peak temperature of our gold nanoparticle ($\Delta T > 350$ K).

So far, we have investigated the impact that temperature dependence of the thermophysical properties and the ITC has on the heating/cooling dynamics of homogeneous nanoparticles. In the following, we extend this analysis and focus on heterogeneous Janus nanoparticles suspended in water. Again, we assumed nanosecond pulsed Gaussian illumination conditions. The Janus particle structure is shown in the inset of Figure 2a. It consists of a polymeric spherical core (we selected PMMA for this study) of radius $R = 40$ nm coated by a gold spherical-semi shell of thickness $\delta = 20$ nm. These materials were chosen because the polymer/water and polymer/gold ITCs are usually low; i.e., the interfacial resistance reduces the heat flow toward the polymer side. Conversely, the gold/water ITC is higher, which translates into a lower interfacial resistance, enabling the heat flow through water. This kind of JNP has been experimentally studied before;[32−35] in fact, the particle geometry and composition studied here are similar to that fabricated by Halas et al.[36,37] Therefore, these experimental studies provided motivation for the system investigated here.

To understand the origin of the JNP thermoplasmonic behavior, we first investigate its electromagnetic response under plane wave illumination and calculate the corresponding absorption cross section (see Figure 2a). This JNP shows a well-defined spectral absorption within the first biological window (NIR-I[38]). This agrees with the calculations and measurements shown in ref 36, which were performed using a constant background refractive index $n = 1.414$ (we use here the water dispersion relation[39]) and an ellipsoidal core made of Polystyrene (PS) instead of PMMA. PS and PMMA have similar optical and thermal properties, and this supports the consistency of our results with the previous studies. Notice that the PMMA−gold semishell resonance can be shifted to the second biowindow (NIR-II[38]) or to other spectral regions of interest, by modifying the core radius and the Au coating thickness or the polymer composition (see Figures S7 and S8 for more details on tunability of the gold−polymer JNP absorption cross section). Importantly, the JNP anisotropy introduces a remarkable absorption dependence with the incidence direction and polarization of the input electromagnetic wave[37] as can be seen in Figure 2b. Here, the absorption cross section of the analyzed hybrid structure is shown when it is transversally illuminated. The absorption features two different peaks as for the situation described in Figure 2a. In this configuration, however, as the electric field is transversal to the largest dimension of the structure, the longitudinal excitation almost disappears. For the same reason, the transversal excitation is enhanced, giving rise to a radically different behavior. This reduction in absorption at the target wavelength translates into a much weaker heating capability (see Figure S9).

Consequently, both the maximum absorption and its spectral position will differ for different incidence conditions and result in a reduction of the maximum achievable temperature. Nevertheless, our main conclusions will still be valid since we are interested in analyzing the impact of the ITC on the JNP transient thermal behavior. For this, it is enough if we consider just normal incidence (see inset in Figure 1). To better characterize and analyze the mechanism that determines the temperature generation, we calculated the near electric and magnetic field spatial distributions for the most beneficial situation (shown in Figure 2c).

The local electric field, $\vec{E}$, upper, and lower maps suggest an accumulation of charges in the gold shell boundaries. This indicates that the electronic motion is following the gold semishell curvature. This is also supported by the two remarkable maxima of the magnetic field, $\vec{H}$, distribution inside the PMMA and outside the gold shell, which emerge from the mentioned electronic motion (see the upper and lower magnetic field maps). This observation agrees with previous studies.[37,40]. Therefore, the resonance can be classified as a magnetic transversal mode, as it is originated from the charge currents in the gold coating.

Now, we consider the thermal transport problem when the JNP is illuminated with a nanosecond pulsed laser. We selected the fluence to target realistic experimental conditions. It is known that fluences of the order of a few tens of millijoules (mJ) per square centimeter can seriously affect the structure of small metallic gold nanoparticles in water due to melting and surface evaporation.[41,42] For gold nanoshells, the mJ threshold also applies, as demonstrated in refs 18,42. This information can be used to estimate the minimum fluence threshold required for shell fragmentation under nanosecond pulsed illumination, $F_{th} = 0.4\ \frac{\mathrm{mJ}}{\mathrm{cm}^2}$. For that reason, all calculations about the thermal behavior of the JNP were performed for fluences under that value. Furthermore, nanosecond pulsed laser with lower fluences ($F = 0.2\frac{mJ}{cm^2}$) in a similar spectral range as the ones shown in Figure 2a have already been employed in previous experiments.[19] This motivated us to consider the fluence $F = 0.2\ \frac{\mathrm{mJ}}{\mathrm{cm}^2}$ for a 1 ns-pulsed laser. Following the approach discussed above, the heat source was modeled as a volumetric heat power density following eq 4.

Figure 3a shows the temperature profiles as a function of time. For our calculations we considered the gold/PMMA and PMMA/water ITCs, 59 and 50 $\frac{\mathrm{MW}}{\mathrm{m}^2\,\mathrm{K}}$,[43,44] respectively, while the value for gold/water ITC was 200 $\frac{\mathrm{MW}}{\mathrm{m}^2\,\mathrm{K}}$.[21] The maximum temperature is reached at $t = 2.4$ ns, followed by a rapid temperature relaxation over time. Also, notice that the gold nanocap is heated first upon illumination, an event that is followed by internal heat transfer to the polymer core and external heat transfer to the solvent. After approximately 2 ns, the temperature inside PMMA gets higher than the gold one, presenting a maximum inside the polymeric core. This can be explained in terms of the low thermal conductivity of the polymer and the low polymer−water ITC, which act as a thermal insulator, resulting in a slower thermal relaxation (see SI movie to get the complete profile temporal study).

https://doi.org/10.1021/acs.jpcc.3c03514
J. Phys. Chem. C 2023, 127, 19152−19158

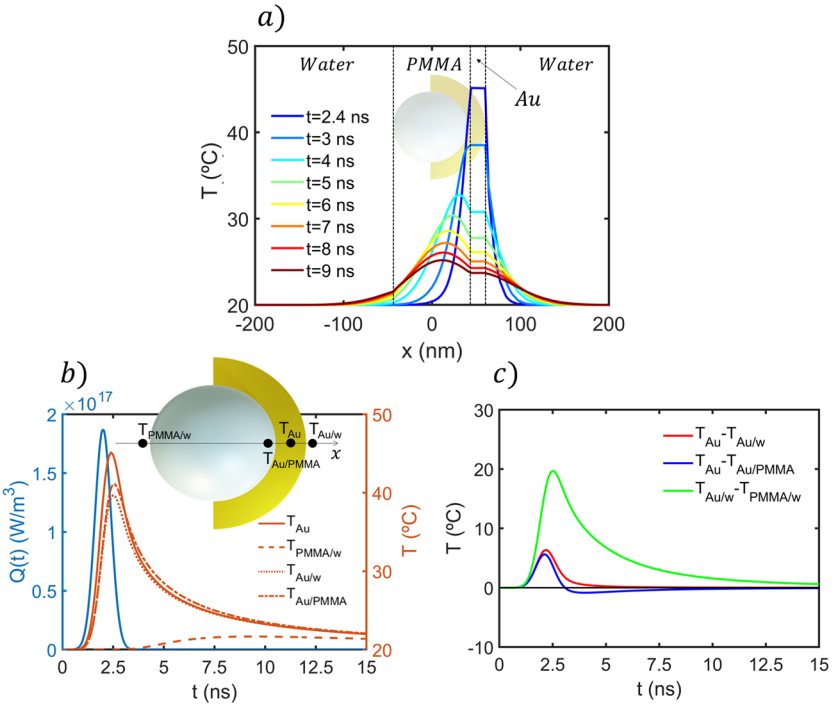

Figure 3. (a) Temperature profiles taken along the x-axis as a function of time. The initial profile is taken at the maximum temperature increase (t = 2.4 ns), so that the cooling process is shown. The vertical lines and the inset display the position of the interfaces. (b) Input heat power density pulse (left plot) and temporal evolution of the temperature (right plot) taken at points T_{Au}, $T_{Au/PMMA}$, $T_{Au/w}$, and $T_{PMMA/w}$ as seen in the upper inset. (c) Temperature contrast as a function of time for $T_{Au} - T_{Au/w}$ (red), $T_{Au} - T_{Au/PMMA}$ (blue), and $T_{Au} - T_{PMMA/w}$ (green). The reference point to calculate the interfacial temperature is placed at 0.1 nm from the surface of the Au or PMMA materials, due to mesh limitations. For bulk gold, T_{Au}, the reference point is located at the center of the gold nanocap.

Figure 3b shows the temperature contrast induced by the interfaces. Here, a comparison of the evolution of temperature is shown at three different interfacial regions ($T_{Au/PMMA}$, $T_{Au/w}$, and $T_{PMMA/w}$, respectively) together with the gold temperature (T_{Au}) taken along the x axis (radial direction PMMA−Au). The interfacial regions are located at 0.1 nm from the surface, except the gold one, T_{Au}, which is located at the center of the gold nanocap. The maximum temperature is reached inside the gold semishell, in the region that is further away from the interfaces. At the gold/polymer interface, a maximum temperature gap of approximately 4 °C can be seen, which is associated with the polymer−gold ITC (59 $\frac{MW}{m^2 K}$). Similarly, a maximum temperature gap of 5.6 °C is present at the gold/water interface due to the considered ITC (200 $\frac{MW}{m^2 K}$). While gold/water features a higher ITC, the larger interfacial temperature jump is connected to the higher heat flux flowing through this interface. However, the time scale of the transient cooling is similar for both interfaces, gold−water and gold−PMMA. One interesting aspect can be remarked at the PMMA/water interface: the temperature increment is much lower (about 1.7 °C with respect to ambient temperature) and increases also slower. It takes more than 9.4 ns to reach the maximum temperature which can be rationalized by considering the low thermal conductivity of PMMA[45] and the low PMMA/Au and PMMA/water ITCs. Indeed, the heat flux calculated at gold−water and PMMA−water interfaces (see Figure S10) shows great asymmetry. In contrast, the rest of the curves reach their peak temperature after 2.4 ns. This translates in a delay of more than 7 ns. It is important because it shows that the temperature contrast achievable with JNP is transferred to the transient process, leading to very large temperature differences across the opposite nanoparticle regions at subnanosecond time scales.

Figure 3c shows that the difference between gold and gold/water or gold/PMMA surface temperatures (red and blue curves) is quite similar. This is supported by both ITCs used here, which also have similar values, 50 vs 59 $\frac{MW}{m^2 K}$. However, the temperature difference ($T_{Au} - T_{Au/PMMA}$) corresponding to the gold/PMMA interface becomes negative after approximately 3 ns, approximately. This can be understood in terms of the thermal properties (including ITC) of materials: gold, the thermoplasmonic heating source, cools down faster through water than PMMA, which is the desired behavior. Thus, the heat flux from gold to PMMA is inverted after 4 ns, with PMMA being hotter that gold, and therefore gold acts a heat sink for the temperature relaxation of the polymer. To get a better idea of the temperature spatial variations generated by the JNP structure, we calculated the temperature contrast between the gold−water and PMMA−water interfaces (green curve in Figure 3c). Considering the low PMMA−water interface temperature, the particle would be suitable for PTT when this contrast is higher than or equal to 10 °C.[46] The results presented in Figure 3c show that the JNP structure can support significant temperature contrasts over 2.2 ns, meaning that a repetition rate shorter than that value might even lead to a stationary contrast over the ideal threshold.

CONCLUSIONS

In summary, we have demonstrated that the thermophysical properties, in particular, the temperature dependence of the solvent specific heat, have a significant impact on the

https://doi.org/10.1021/acs.jpcc.3c03514
J. Phys. Chem. C 2023, 127, 19152−19158

thermoplasmonic calculations of JNPs when pulsed illumination is used. The optical properties are affected by temperature, leading to a reduction of the structure absorption capabilities, especially at high temperatures. Although it affects the interfacial temperatures, the temperature contrast associated with the anisotropic interfacial thermal conductance remains almost invariant. This conductance, often neglected in continuum calculations, plays a crucial role in determining the dynamics of a nanoparticle upon illumination as well as on the dynamics of the subsequent relaxation process. Hence, we conclude that the ITC is an important variable that must be considered to accurately describe the thermoplasmonic response of nanomaterials. We investigated the transient behavior, under the same pulsed illumination conditions, of a polymer/gold core/semishell nanoparticle, a nanomaterial that has been studied in previous experimental works with the same geometry ((Au shell thickness, PMMA radius) = (20, 40) nm). We found that this JNP offers a maximum temperature increase of more than 10 °C with a high temperature difference between the polymer and metallic sides of the nanoparticles, hence providing asymmetric heating, which is potentially relevant to PTT applications. We also found that the maximum temperature contrast was achieved at 2.4 ns, and we expect that higher temperatures can be achieved using nanosecond light pulses with repetition rates below 2.4 ns (Figure S11). This single particle study can be representative of a highly diluted sample; however, before these results can be taken to practice, further studies need to be performed for relatively dense colloids to explore the influence that collective effects may have in PTT. The potential of these Janus particle colloids stem from their intrinsic capacity to generate thermal asymmetry and undergo selective biofunctionalization.[47,48] Through this synergistic combination, the randomly administrated particles will be more likely to adhere to cells through their hotter region. This offers a dual benefit: enhanced heating efficiency due to the majority of thermal energy channeled toward the target cells and thermal insulation of the surrounding tissue. Furthermore, the model we have proposed here can be used to analyze any JNP geometry taking into consideration time dependence thermophysical properties and the ITC. Our work can also be useful in other areas, beyond PTT applications, and might provide input to develop novel Janus architectures to reach efficient heating control at the nanoscale, an objective of particular interest among the thermoplasmonics community.

■ ASSOCIATED CONTENT

Supporting Information

The Supporting Information is available free of charge at https://pubs.acs.org/doi/10.1021/acs.jpcc.3c03514.

Additional computational details, materials, descriptions, including the optimization of the proposed hybrid nanoheater and the modeling of the temperature dependent permittivity of gold (PDF)

Movie containing the temporal evolution of the Janus structure thermal profile (MP4)

■ AUTHOR INFORMATION

Corresponding Authors

Fernando Bresme − *Department of Chemistry, Molecular Sciences Research Hub, Imperial College London, London W12 0BZ, U.K.*; orcid.org/0000-0001-9496-4887; Email: f.bresme@imperial.ac.uk

Pablo Albella − *Group of Optics, Department of Applied Physics, University of Cantabria, 39005 Santander, Spain*; orcid.org/0000-0001-7531-7828; Email: pablo.albella@unican.es

Author

Javier González-Colsa − *Group of Optics, Department of Applied Physics, University of Cantabria, 39005 Santander, Spain*; orcid.org/0000-0003-3583-987X

Complete contact information is available at: https://pubs.acs.org/10.1021/acs.jpcc.3c03514

Notes

The authors declare no competing financial interest.

■ ACKNOWLEDGMENTS

We gratefully acknowledge financial support from Spanish national project INMUNOTERMO (No. PGC2018-096649-B-I) and the UK Leverhulme Trust (Grant No. RPG-2018-384). J.G.-C. thanks the Ministry of Science and Innovation of Spain for his FPI grant, and P.A. acknowledges funding for a Ramon y Cajal Fellowship (Grant No. RYC-2016-20831).

■ REFERENCES

(1) Casagrande, C.; Fabre, P.; Raphaël, E.; Veyssié, M. Janus Beads": Realization and Behaviour at Water/Oil Interfaces. *Europhys. Lett.* **1989**, *9* (3), 251−255.

(2) Bickel, T.; Zecua, G.; Würger, A. Polarization of Active Janus Particles. *Phys. Rev. E Stat Nonlin Soft Matter Phys.* **2014**, *89* (5), No. 050303.

(3) Olarte-Plata, J. D.; Bresme, F. Orientation of Janus Particles under Thermal Fields: The Role of Internal Mass Anisotropy. *J. Chem. Phys.* **2020**, *152* (20), No. 204902.

(4) Bresme, F.; Olarte-Plata, J. D.; Chapman, A.; Albella, P.; Green, C. Thermophoresis and Thermal Orientation of Janus Nanoparticles in Thermal Fields. *Eur. Phys. J. E* **2022**, *45* (7), 59.

(5) Hirsch, L. R.; Stafford, R. J.; Bankson, J. A.; Sershen, S. R.; Rivera, B.; Price, R. E.; Hazle, J. D.; Halas, N. J.; West, J. L. Nanoshell-Mediated near-Infrared Thermal Therapy of Tumors under Magnetic Resonance Guidance. *Proc. Natl. Acad. Sci. U. S. A.* **2003**, *100* (23), 13549−13554.

(6) Lal, S.; Clare, S. E.; Halas, N. J. Nanoshell-Enabled Photothermal Cancer Therapy: Impending Clinical Impact. *Acc. Chem. Res.* **2008**, *41* (12), 1842−1851.

(7) Jaque, D.; Martínez Maestro, L.; del Rosal, B.; Haro-Gonzalez, P.; Benayas, A.; Plaza, J. L.; Martín Rodríguez, E.; García Solé, J. Nanoparticles for Photothermal Therapies. *Nanoscale* **2014**, *6* (16), 9494−9530.

(8) González-Colsa, J.; Serrera, G.; Saiz, J. M.; Ortiz, D.; González, F.; Bresme, F.; Moreno, F.; Albella, P. Gold Nanodoughnut as an Outstanding Nanoheater for Photothermal Applications. *Opt Express* **2022**, *30* (1), 125.

(9) González-Colsa, J.; Olarte-Plata, J. D.; Bresme, F.; Albella, P. Enhanced Thermo-Optical Response by Means of Anapole Excitation. *J. Phys. Chem. Lett.* **2022**, *13* (26), 6230−6235.

(10) Olarte-Plata, J. D.; Gabriel, J.; Albella, P.; Bresme, F. Spatial Control of Heat Flow at the Nanoscale Using Janus Particles. *ACS Nano* **2022**, *16* (1), 694−709.

(11) González-Colsa, J.; Franco, A.; Bresme, F.; Moreno, F.; Albella, P. Janus-Nanojet as an Efficient Asymmetric Photothermal Source. *Sci. Rep* **2022**, *12* (1), 14222.

(12) Amendola, V.; Pilot, R.; Frasconi, M.; Maragò, O. M.; Iatì, M. A. Surface Plasmon Resonance in Gold Nanoparticles: A Review. *J. Phys.: Condens. Matter* **2017**, *29* (20), No. 203002.

(13) Govorov, A. O.; Richardson, H. H. Generating Heat with Metal Nanoparticles. *Nano Today* **2007**, *2* (1), 30−38.
(14) Baffou, G.; Quidant, R.; García De Abajo, F. J. Nanoscale Control of Optical Heating in Complex Plasmonic Systems. *ACS Nano* **2010**, *4* (2), 709−716.
(15) Jauffred, L.; Samadi, A.; Klingberg, H.; Bendix, P. M.; Oddershede, L. B. Plasmonic Heating of Nanostructures. *Chem. Rev.* **2019**, *119* (13), 8087−8130.
(16) Carroll, L.; Humphreys, T. R. LASER-Tissue Interactions. *Clin Dermatol* **2006**, *24* (1), 2−7.
(17) Metwally, K.; Mensah, S.; Baffou, G. Fluence Threshold for Photothermal Bubble Generation Using Plasmonic Nanoparticles. *J. Phys. Chem. C* **2015**, *119* (51), 28586−28596.
(18) Akchurin, G.; Khlebtsov, B.; Akchurin, G.; Tuchin, V.; Zharov, V.; Khlebtsov, N. Gold Nanoshell Photomodification under a Single-Nanosecond Laser Pulse Accompanied by Color-Shifting and Bubble Formation Phenomena. *Nanotechnology* **2008**, *19* (1), No. 015701.
(19) Lukianova-Hleb, E. Y.; Lapotko, D. O. Influence of Transient Environmental Photothermal Effects on Optical Scattering by Gold Nanoparticles. *Nano Lett.* **2009**, *9* (5), 2160−2166.
(20) Zhang, X.; Qiu, J.; Zhao, J.; Li, X.; Liu, L. Complex Refractive Indices Measurements of Polymers in Infrared Bands. *J. Quant Spectrosc Radiat Transf* **2020**, *252*, No. 107063.
(21) Olarte-Plata, J. D.; Bresme, F. Thermal Conductance of the Water-Gold Interface: The Impact of the Treatment of Surface Polarization in Non-Equilibrium Molecular Simulations. *J. Chem. Phys.* **2022**, *156* (20), No. 204701.
(22) Magnozzi, M.; Ferrera, M.; Mattera, L.; Canepa, M.; Bisio, F. Plasmonics of Au Nanoparticles in a Hot Thermodynamic Bath. *Nanoscale* **2019**, *11* (3), 1140−1146.
(23) Buffat, P.; Borel, J.-P. Size Effect on the Melting Temperature of Gold Partlcles. *Phys. Rev. A (Coll Park)* **1976**, *13* (6), 2287−2298.
(24) Chen, J.; Fan, X.; Liu, J.; Gu, C.; Shi, Y.; Zheng, W.; Singh, D. J. Interior Melting of Rapidly Heated Gold Nanoparticles. *J. Phys. Chem. Lett.* **2021**, *12* (34), 8170−8177.
(25) Chen, X.; Munjiza, A.; Zhang, K.; Wen, D. Molecular Dynamics Simulation of Heat Transfer from a Gold Nanoparticle to a Water Pool. *J. Phys. Chem. C* **2014**, *118* (2), 1285−1293.
(26) Lide, D. R.; Baysinger, G.; Berger, L. I.; Goldberg, R. N.; Kehiaian, H. V; Kuchitsu, K.; Roth, D. L.; Zwillinger, D. *CRC Handbook of Chemistry and Physics*; CRC Press: Boca Raton, FL, 2005.
(27) Alabastri, A.; Toma, A.; Malerba, M.; De Angelis, F.; Proietti Zaccaria, R. High Temperature Nanoplasmonics: The Key Role of Nonlinear Effects. *ACS Photonics* **2015**, *2* (1), 115−120.
(28) Shen, P.-T.; Sivan, Y.; Lin, C.-W.; Liu, H.-L.; Chang, C.-W.; Chu, S.-W. Temperature- and Roughness-Dependent Permittivity of Annealed/Unannealed Gold Films. *Opt Express* **2016**, *24* (17), 19254.
(29) Un, I. W.; Sivan, Y. Thermo-Optic Nonlinearity of Single Metal Nanoparticles under Intense Continuous Wave Illumination. *Phys. Rev. Mater.* **2020**, *4* (10), No. 105201.
(30) Gurwich, I.; Sivan, Y. Metal Nanospheres under Intense Continuous-Wave Illumination: A Unique Case of Nonperturbative Nonlinear Nanophotonics. *Phys. Rev. E* **2017**, *96* (1), No. 012212.
(31) Sivan, Y.; Chu, S. W. Nonlinear Plasmonics at High Temperatures. *Nanophotonics* **2017**, *6* (1), 317−328.
(32) Suzuki, D.; Kawaguchi, H. Janus Particles with a Functional Gold Surface for Control of Surface Plasmon Resonance. *Colloid Polym. Sci.* **2006**, *284* (12), 1471−1476.
(33) Rashidi, A.; Issa, M. W.; Martin, I. T.; Avishai, A.; Razavi, S.; Wirth, C. L. Local Measurement of Janus Particle Cap Thickness. *ACS Appl. Mater. Interfaces* **2018**, *10* (37), 30925−30929.
(34) Razavi, S.; Hernandez, L. M.; Read, A.; Vargas, W. L.; Kretzschmar, I. Surface Tension Anomaly Observed for Chemically-Modified Janus Particles at the Air/Water Interface. *J. Colloid Interface Sci.* **2020**, *558*, 95−99.
(35) Rodríguez-Fernández, D.; Liz-Marzán, L. M. Metallic Janus and Patchy Particles. *Particle and Particle Systems Characterization* **2013**, *30* (1), 46−60.
(36) Mirin, N. A.; Halas, N. J. Light-Bending Nanoparticles. *Nano Lett.* **2009**, *9* (3), 1255−1259.
(37) King, N. S.; Li, Y.; Ayala-Orozco, C.; Brannan, T.; Nordlander, P.; Halas, N. J. Angle- and Spectral-Dependent Light Scattering from Plasmonic Nanocups. *ACS Nano* **2011**, *5* (9), 7254−7262.
(38) Hemmer, E.; Benayas, A.; Légaré, F.; Vetrone, F. Exploiting the Biological Windows: Current Perspectives on Fluorescent Bioprobes Emitting above 1000 Nm. *Nanoscale Horiz* **2016**, *1* (3), 168−184.
(39) Hale, G. M.; Querry, M. R. Optical Constants of Water in the 200-Nm to 200-Mm Wavelength Region. *Appl. Opt.* **1973**, *12* (3), 555−563.
(40) Cortie, M.; Ford, M. A Plasmon-Induced Current Loop in Gold Semi-Shells. *Nanotechnology* **2007**, *18* (23), No. 235704.
(41) Fales, A. M.; Vogt, W. C.; Pfefer, J.; Ilev, I. K. Quantitative Evaluation of Nanosecond Pulsed Laser-Induced Photomodification of Plasmonic Gold Nanoparticles. *Sci. Rep* **2017**, *7* (1), 15704.
(42) Aguirre, C. M.; Moran, C. E.; Young, J. F.; Halas, N. J. Laser-Induced Reshaping of Metallodielectric Nanoshells under Femtosecond and Nanosecond Plasmon Resonant Illumination. *J. Phys. Chem. B* **2004**, *108* (22), 7040−7045.
(43) Sandell, S.; Maire, J.; Chávez-ángel, E.; Torres, C. M. S.; Kristiansen, H.; Zhang, Z.; He, J. Enhancement of Thermal Boundary Conductance of Metal−Polymer System. *Nanomaterials* **2020**, *10* (4), 670.
(44) Lervik, A.; Bresme, F.; Kjelstrup, S. Heat Transfer in Soft Nanoscale Interfaces: The Influence of Interface Curvature. *Soft Matter* **2009**, *5* (12), 2407−2414.
(45) Assael, M. J.; Botsios, S.; Gialou, K.; Metaxa, I. N. Thermal Conductivity of Polymethyl Methacrylate (PMMA) and Borosilicate Crown Glass BK7. *Int. J. Thermophys* **2005**, *26* (5), 1595−1605.
(46) Chu, K. F.; Dupuy, D. E. Thermal Ablation of Tumours: Biological Mechanisms and Advances in Therapy. *Nat. Rev. Cancer* **2014**, *14* (3), 199−208.
(47) Fan, J.-B.; Song, Y.; Liu, H.; Lu, Z.; Zhang, F.; Liu, H.; Meng, J.; Gu, L.; Wang, S.; Jiang, L. A General Strategy to Synthesize Chemically and Topologically Anisotropic Janus Particles. *Sciences Advances* **2017**, *3* (6), No. e1603203.
(48) Kadam, R.; Zilli, M.; Maas, M.; Rezwan, K. Nanoscale Janus Particles with Dual Protein Functionalization. *Particle and Particle Systems Characterization* **2018**, *35* (3), No. 1700332.

https://doi.org/10.1021/acs.jpcc.3c03514
J. Phys. Chem. C 2023, 127, 19152−19158